AMS Home   Journals Home   Journal Archive   Subscribe   For Authors   Help   Advanced Search   Search   Go

Full Text View

The Seasonal Heat Budget of the North Pacific: Net Heat Flux and Heat Storage Rates (1950–1990)

John R. Moisan[*] **and Pearn P. Niiler**

Physical Oceanography Research Division, Scripps Institution of Oceanography, La Jolla, California

ABSTRACT

A new estimate of the heat budget for the North Pacific Ocean is presented in this paper. The seasonal net heat flux and heat storage rates were calculated for the North Pacific Ocean from 1950 to 1990 on a spatial resolution of $5° \times 5°$. Temperature profiles from the National Ocean Data Center were used to calculate the heat storage rates. Satellite remotely sensed solar irradiance and ship marine weather reports from the Comprehensive Ocean–Atmosphere Data Set were used to calculate the net surface heat flux. Heat storage rates were calculated as the time rate of change of the heat content integrated from the surface down to the isotherm that was 1°C less than the coldest locally observed wintertime sea surface temperature, which was defined as the locally observed wintertime ventilation isotherm. The monthly climatology of the $5° \times 5°$ resolution net heat flux was balanced by the heat storage rate for most regions of the North Pacific. To achieve this balance the net heat flux was calculated using the Liu et al. formulations for latent and sensible heat exchange and a modified version of the Reed cloud correction for solar insolation. The root-mean-square error in the difference between the net heat flux and heat storage rate climatologies was calculated at 40 W m^{-2}. When the individual temperature profiles from the northeastern portion of the basin were normalized to the local 300-m mean temperature, thereby removing some of the potential local changes caused by barotropic variability of water motion, the root-mean-square error in this region was further reduced to 20 W m^{-2} and the large-scale semiannual periodicity in the difference observed in the subtropics was removed. This normalization process may have removed some of the basin-scale variability in the horizontal heat advection. An estimate of the northward heat transport was calculated by integrating the annual mean net heat flux over the North Pacific. The resulting heat transport values were closer to actual northward heat transport estimates made at 10°, 24°, 35°, and 47°N, than previous ocean heat flux estimates. The bias in the data was estimated to be less than 7% by comparing the demeaned seasonal cycle of the net heat flux with that of the heat storage rates. The annual mean net heat flux was then used with the 7% bias and the 20 W m^{-2} uncertainty to calculate a more constrained error envelope for the annual mean northward heat transport in the North Pacific.

Options:
- Create Reference
- Email this Article
- Add to MyArchive
- Search AMS Glossary

Search CrossRef for:
- Articles Citing This Article

Search Google Scholar for:
- John R. Moisan
- Pearn P. Niiler

1. Introduction

The flux of heat across the ocean–atmosphere interface is an important link between the ocean and atmosphere systems. The current trend of ocean general circulation models (OGCMS) is to use estimates of these fluxes to seasonally force ocean system models (Semtner and Chervin 1992). A recent comparison of model results from several tropical OGCMS showed that the simulated sea surface temperature (SST) in the western Pacific was too warm in all the models. This consistent overestimation of the SST is believed to result from inaccuracies in the climatological heat flux estimates (Stockdale et al. 1993). An improvement in the estimate of these fluxes is needed if we are to accurately model, and thereby understand and potentially predict, the interactions between the ocean and atmosphere systems.

Studies on the ocean–atmosphere heat flux have focused on the climatological variability and annual mean heat flux terms for the North Atlantic (Bunker 1976; Isemer and Hasse 1987), North Pacific (Wyrtki 1965; Yan et al. 1995), tropical Atlantic (Hastenrath and Lamb 1977, 1978), and the global ocean (Esbensen and Kushnir 1981; Hsiung 1985; Oberhuber 1988). An early estimate of the annual mean heat flux in the North Pacific Ocean, using data collected from 1947 to 1960, indicates that the North Pacific Ocean transports heat southward across the equator so as to balance the net heat gain of 0.14 petawatts (Wyrtki 1965). Unlike the Wyrtki (1965) estimate, the results from more recent atlases indicate that the North Pacific Ocean is a basin where heat is transported north across the equator (Esbensen and Kushnir 1981; Hsiung 1985; Oberhuber 1988). The major difference between these estimates is in the formulation of the cloud effects on the solar shortwave heat flux and the determination of the bulk transfer coefficients for the latent and sensible heat flux.

There are many methods to estimate the bulk latent and sensible heat transfer rates using surface meteorological observations. Currently, there is no single, universally accepted bulk transfer scheme (Blanc 1985). Also, estimates of the solar shortwave heat flux vary significantly depending on the method used to parameterize the effect of clouds (Dobson and Smith 1988). Thus, it has been difficult to choose which cloud correction scheme or which bulk latent and sensible heat flux formula to use in order to estimate the heat fluxes.

Relatively simple models of solar shortwave radiation can give accurate estimates of the heat flux during clear sky conditions. However, much of the ocean is covered by clouds for a significant portion of time, which decrease and even sometimes locally increase the amount of shortwave energy incident upon the ocean surface. In recent years, there has been a large increase in the amount of both remotely sensed data (Liu et al. 1992; Bishop and Rossow 1991; Chertock et al. 1992; Frouin and Chertock 1992) and measured data (Niiler et al. 1997, submitted to *J. Geophys. Res.*) on the components of the ocean heat budget. This increase in available data is important because such measurements were historically impossible to acquire at synoptic time and space scales. With remotely sensed data, it is now possible to obtain better parameterizations of the net shortwave energy term, which until recently has been been difficult to estimate.

The seasonal variability of the ocean–atmosphere net heat flux is balanced locally by the amount of heat stored in the ocean (Gill and Niiler 1973). However, because of the large vertical motions associated with the isotherms or thermocline, any measurement of the local heat storage rates must take into account this process (Stevenson and Niiler 1983). Validation or selection between those heat flux parameterizations that have been proposed in the literature may be possible by using calculated estimates of the local heat storage rates.

The objectives of this paper are to calculate the monthly mean heat storage rates, net heat flux, and annual northward heat transport for the North Pacific Ocean from 1950 to 1990. The choice of which latent and sensible bulk parameterization and shortwave heat flux estimate to use in calculating the heat flux was made by comparing the seasonal cycle of the net heat flux from the various estimates against the calculated seasonal heat storage rates. The resulting annual mean heat flux estimates were then used to estimate the northward heat transport for the North Pacific. The second section presents the methods used to calculate both the net heat flux and heat storage rates for the North Pacific from 1950 to 1990. The sections following the methods present the results of the (i) 40-yr time series estimates at several locations, Ocean Weather Station (OWS) Papa and November; (ii) seasonal cycles; (iii) annual means;(iv) uncertainty analysis; and (v) northward heat transport. The final section presents a discussion of the results.

The results show that by using the calculated monthly mean heat storage rates a choice can be made between the various latent, sensible, and shortwave heat flux estimates. The new estimate of heat flux in the North Pacific has less than a 7% bias when compared against the heat storage rates. The resulting northward heat transport compares well with several direct estimates from various latitudes.

2. Heat budget calculation

The upper-ocean heat budget was calculated using the three-dimensional heat conservation equation,

$$\rho c_p \left(h \frac{\partial T_a}{\partial t} + h \mathbf{v}_a \cdot \nabla T_a \right) = Q_{\text{net}}, \qquad (1)$$

where ρ is the mean density of seawater, c_p is the specific heat of seawater, h is the depth of a chosen isotherm across which there is a minimal heat transfer rate and from which the depth-averaged temperature T_a and depth-averaged horizontal velocity $\mathbf{v}_a$ were calculated, ∇ is the horizontal gradient operator ($\nabla \equiv \partial/\partial x, \partial/\partial y$), and Q_{net} is the net heat flux across the ocean surface. A formal derivation of this equation is presented in the appendix.

Monthly mean values of the heat storage rate and net ocean heat flux were calculated for the global ocean at a spatial resolution of 5° × 5° and a time period spanning 1950 to 1990. This period was chosen because it brackets the time during which temperature profiles and meteorological data are available and changes in the globally averaged seasonal variability and annual mean of the meteorological observations are minimal. The grid is bounded by the 5° latitude by 5° longitude lines. The data and methods used to calculate each of these ocean heat balance terms are presented below.

a. Heat storage rate

The heat storage rate (HSR),

$$\rho c_p \left(h \frac{\partial T_a}{\partial t} \right), \qquad (2)$$

was calculated using monthly averaged data,

$$\rho c_p \left(\langle h \rangle \frac{\partial \langle T_a \rangle}{\partial t} \right), \qquad (3)$$

where $\langle h \rangle$ and $\langle T_a \rangle$ denote the monthly mean values for the depth of the chosen isotherm and the depth-integrated temperature, respectively. The derivatives were calculated using either centered, forward, or backward differencing in time depending upon the availability of monthly mean data.

Ocean temperature data were obtained from the NODC's global ocean temperature and salinity profiles dataset, which contains over 1.57 million profiles of salinity and/or temperature from the Pacific Ocean from 1900 to 1990. The time series from 1950 to 1990 of the monthly mean vertically averaged temperature $\langle T_a \rangle$ was calculated along with the standard deviation (std dev) and 95% confidence interval (C.I.) by integrating each temperature profile down to a specified isotherm. The time series of the monthly mean integration depth $\langle h \rangle$ was also recorded along with its std dev and 95% C.I. Integrating to a specific isotherm rather than to a constant depth removed much of the variance caused by vertical motion of the thermocline due to the passage of mesoscale eddies or Rossby waves (Fig. 1 ⊙■).

Choosing which isotherm to integrate to was an important consideration for calculating heat storage rates. If the chosen isotherm was too cold, fewer temperature profiles were available to integrate because the profiles did not drop to temperatures equal to or less than the chosen isotherm and therefore were unusable. If the chosen isotherm was too warm, the integration may have missed heat stored below the chosen isotherm.

The sensitivity of $\langle h \rangle$, $\langle T_a \rangle$, and $\rho c_p \langle h \rangle (\partial \langle T_a \rangle / \partial t)$ to changes in the isotherm to which the data were integrated is shown in Fig. 2 ⊙■. While both $\langle h \rangle$ and $\langle T_a \rangle$ were sensitive to changes in isotherm choice, the heat storage rate, $\rho c_p \langle h \rangle (\partial \langle T_a \rangle / \partial t)$, was much less sensitive. The criterion used to estimate the isotherm was that it was to be the coldest surface temperature observed within the particular 5° × 5° bin and between the time span of the available data. This temperature minimum can be viewed as the mixed layer temperature during deep winter ventilation of the water column. The assumption made here was that the isotherms, to which the integrations were performed, were well below the region of influence of net heating via solar radiation flux and upper-ocean mixing processes. In practice, however, in order to obtain a smoothly varying isotherm field for calculating the heat storage rates, the isotherms were set to the coldest observed temperature from the Oberhuber (1988) atlas, which contains climatological means of sea surface temperature using data from the Comprehensive Ocean–Atmosphere Data Set (COADS) (Slutz et al. 1985; Woodruff et al. 1987). Because the Oberhuber atlas contains climatological data, the final chosen integration isotherms were set one degree below the coldest locally observed sea surface temperature. This definition for ventilation mixed layer depth is similar to the one used by Suga and Hanawa (1990) for a mixed layer.

After the available data were used to calculate the time series of both $\langle T_a \rangle$ and $\langle h \rangle$, all data that contained a 95% C.I. (C.I. $= 1.96 s / (n)^{1/2}$) larger than the mean, for either $\langle T_a \rangle$ or $\langle h \rangle$ were rejected. The resulting time series of the local heat storage rates, $\rho c_p \langle h \rangle (\partial \langle T_a \rangle / \partial t)$, was then calculated using the remaining data.

Observations of the monthly mean temperature profiles show significant seasonal temperature variations below 200 m, some as high as 2°C. The temperature profiles at 200 m vary little with depth and show colder temperatures occurring in the summer months, at a time when the sea surface temperature is maximum. Estimates from simple heat diffusion models suggest that these out-of-phase temperature relationships are an order of magnitude too large to be caused by vertical diffusion alone (Kenyon 1983). However, because the Kuroshio Current System is a region of high shear, simple diffusion models may underestimate the role of vertical diffusion in determining the seasonal cycle of the temperature at depth in the Kuroshio. These deep water changes in the temperature profile can alter the depth of the isotherm to which $\langle T_a \rangle$ and $\langle h \rangle$ are calculated, thus the temperature profiles from the NODC dataset north of 20°N were normalized to the 300-m mean temperature observed within each 5° × 5° grid before they were integrated to calculate both $\langle h \rangle$ and $\langle T_a \rangle$ (Fig. 3 ⊙■).

The temperatures between the upper-ocean mixed layer and 500 m vary equally at all depths. Because of this, it is difficult to distinguish whether the variability is caused by horizontal or vertical advection processes. This variability can also be explained by the theory that the variability in barotropic currents move both the horizontal currents and isotherms horizontally (Gill and Niiler 1973).

The normalization of the individual temperature profiles removed a significant portion of both the annual and interannual horizontal heat advection signatures from the calculation. Some of this variability was thought to be associated with the annual and interannual displacement of the wall of the Kuroshio Current System, which is often located using the 12°C isotherm at 300 m (Mizuno and White 1983).

b. Net heat flux

The net heat flux (NHF) across the ocean–atmosphere interface can be written as

$$Q_{\text{net}} = Q_I - Q_l - Q_s - Q_b, \quad (4)$$

where Q_I is the incoming solar shortwave irradiance, Q_l is the upward latent heat flux, Q_s is the upward sensible heat flux, and Q_b is the net longwave back radiation. A description of the methods used to calculate each of the net heat flux terms follows.

1) INCOMING SOLAR SHORTWAVE RADIATION

Monthly mean net surface solar irradiance was calculated using two methods. The first used data derived from the International Satellite Cloud Climatology Project (ISCCP) (Rossow et al. 1985) and a radiative transfer model to create a 2.5° × 2.5° resolution dataset spanning the period of July 1983 through June 1991, inclusive (Bishop and Rossow 1991). In the second method, monthly mean cloud data from the COADS were used in conjunction with a wavelength-dependent clear sky solar irradiance model (Bird 1984) and a cloud correction algorithm (Reed 1977) to produce an estimate of the surface solar irradiance for the period of January 1950 through December 1992. The monthly mean cloud data were extracted from the "Monthly Summaries Trimmed Group" Release 1 and 1a of the COADS. This dataset uses marine weather observations from 1854 to 1992 to calculate monthly averaged data on several ocean/atmosphere values such as sea surface temperature, air temperature, cloud cover, relative humidity, and wind speed at a resolution of 2° × 2°. Both incident shortwave radiation estimates were linearly interpolated onto the 5° × 5° grid used in this study. Estimates of the absorbed solar irradiance were obtained using the incident shortwave estimates and were corrected for the surface albedo effect using a mean ocean surface albedo of 0.06 (Payne 1972).

While a comparison between the climatological means of these two datasets shows a general agreement (Fig. 4a ⊙━), a comparison of the climatologies derived from these two datasets (not shown) shows a significant ($\pm\sim 20$ W m^{-2}) spatial variability between the two estimates.

Therefore, a nonlinear cloud correction algorithm (modified after Reed 1977) was used with the Bird (1984) clear-sky solar radiation model and the COADS cloud data. With this algorithm, the fraction of surface shortwave solar radiation to clear sky radiation can be written as

$$\frac{Q_I}{Q_0} = (1 - \alpha)(1 - a_1 + a_2 \sin(H))$$

$$\times \{1 - [C(a_3 + a_4 \cos(H))]\}, \quad (5)$$

where α is the ocean surface albedo (0.06 for this study), H is the solar altitude in radians, and C is the COADS monthly mean cloud amount in tenths. The four coefficients, a_1 through a_4, were fit independently to each 5° × 5° grid bin using the Bishop and Rossow (1991) estimate and the COADS cloud data for July 1983 through June 1991. Each coefficient, a_1 through a_4, ranged between −2 and 2. The spatial variability in the coefficients is caused by changes in cloud type and cover. Similar cloud correction algorithms have been obtained using data from OWS Papa and then extrapolated into other ocean regions (Smith and Dobson 1984). However, given the wide geographic variability in the dominant cloud type (the cumulonimbus clouds in the intertropical convergence zone and the cumulus clouds in the trade wind belt), extrapolating these local cloud correction algorithms to other ocean regions is inappropriate. A comparison of the Bishop and Rossow (1991) data to the model fit (5) is shown in Fig. 4b ⊙━. The derived coefficients were then used with the full 40 years of COADS cloud data to extrapolate the solar shortwave estimate over the entire 40-yr time span of this study. A potential deficiency of using the model and cloud correction to estimate the full 40 years of solar radiance is that the cloud correction algorithm is unable to account for shifts in cloud type that may have occurred in the years outside of the Bishop and Rossow (1991) dataset.

2) LATENT AND SENSIBLE HEAT FLUX

Both latent, Q_l, and sensible, Q_s, heat flux estimates were calculated using monthly mean $5° \times 5°$ resolution COADS data and the formulations

$$Q_l = \rho L C_E \{w\Delta q\} \qquad (6)$$

and

$$Q_s = \rho C_p C_H \{w\Delta T\}, \qquad (7)$$

where ρ is the air density, L is the latent heat per unit mass, and C_p is the specific heat of air at constant pressure. These terms were calculated with the available COADS data and standard algorithms for thermodynamic atmospheric calculations (Schlatter and Baker 1981). The terms C_E and C_H are the bulk transfer coefficients for latent and sensible heat, respectively, which were estimated using several bulk transfer schemes. The term $\{w\Delta q\}$ is the monthly mean of the product of the wind speed magnitude and the difference between the surface saturation humidity and air humidity. The term $\{w\Delta T\}$ is the monthly mean of the product of the wind speed magnitude and the difference between the sea surface temperature and the air temperature. The use of monthly mean values or climatology versus synoptic data of atmospheric–ocean data has been investigated by Fissel et al. (1977) and Ledvina et al. (1993). The COADS dataset reduces the effect of using monthly mean estimates by furnishing the mean of the products of the observations needed to calculate the latent and sensible heat fluxes. A more detailed discussion of this sampling problem is presented in Cayan (1992a). A comparison of ten different bulk transfer coefficient schemes (Blanc 1985) shows that the differences using the entire historical archive of schemes results in a maximum variation near 45%. When more modern and time proven schemes are utilized, a 10% difference can be obtained. Which modern scheme should be used? A comparison between the latent and sensible heat flux estimates of several different modern schemes (Figs. 5 ⊙ and 6 ⊙, respectively) shows that the variability between schemes relative to the observed variability within each scheme is less than 15% for the latent heat flux and much less for the sensible heat flux estimates. The scheme used in this paper is the bulk parameterization method of Liu et al. (1979). This scheme uses monthly mean values of wind, sea surface temperature, air temperature, and relative humidity from the COADS dataset to obtain the bulk transfer coefficients. Esbensen and Reynolds (1981) show that the use of monthly mean data to estimate latent and sensible heat fluxes gives a relative mean error of near 10%. The Liu et al. (1979) scheme was chosen because 1) the resulting seasonal net heat flux estimates had less bias when compared to the seasonal heat storage rates and 2) it compared favorably against the other schemes tested (e.g., Large and Pond 1982; Isemer and Hasse 1987) for both the latent and sensible heat flux estimates.

3) LONGWAVE BACK RADIATION

The net outgoing flux of longwave radiation from the sea surface was calculated using the parameterization of Bunker (1976). The formulation is written as

$$Q_b = \varepsilon\sigma\langle T^4_A\rangle(0.254 - 0.00495 e_A)(1 - cn) + 4\varepsilon\sigma T^3_A(T_S - T_A), \quad (8)$$

where $\varepsilon = 0.96$ is the emissivity of the surface, σ is the Stefan–Boltzmann constant, T_A is the air temperature, e_A is the water vapor pressure in millibars, c is a latitude-dependent cloud correction factor, n is the fraction of total cloud cover, and T_S is the sea surface temperature. The air temperature, sea surface temperature, water vapor pressure, and cloud cover data were obtained from the COADS.

3. 40-yr time series: 1950–1990

There is a lack of XBT/CTD and sea surface meteorological data on the World Ocean. Because of this, in the North Pacific only 26% of the 40-yr monthly mean time series had concurrent upper-ocean HSR and NHF estimates. Most of this data, 46%, was obtained after 1970, primarily due to the development and use of the XBT. As an example, the two time series of the NHF and HSR [calculated using data from the $5° \times 5°$ grids, which contain the data from OWS Papa (Fig. 7 ⊙) and OWS November (Fig. 8 ⊙)] show significant periods during which no data were collected.

There are several processes used in other studies to fill in missing data points and/or filter the time series. Yan et al. (1995) employed a linear interpolation scheme to estimate missing values of $\langle T_a\rangle$ and $\langle h\rangle$ and then filtered the time series with a 16–8 month bandpass filter to suppress spikes within the time series. Such data processing does little to enhance the available information within the dataset. Because of this, the time series data were not postprocessed.

It is evident from the time series plots (Figs. 7 ⊙ and 8 ⊙) that both the NHF and HSR covary and are dominated by seasonal cycles. Also, the differences between the actual time series and the monthly mean climatologies are small. Further analysis of the heat flux residuals from such a time series has been previously done by Cayan (1992a, b, c) for the latent and sensible heat flux components, calculated with the Large and Pond (1982) scheme. Because this paper focused on the seasonal cycles, the analysis of the residuals from the HSR and NHF data was not done.

4. Seasonal cycles

A comparison of the difference between two methods to calculate the HSR is shown in Fig. 9 ⊙. The seasonal HSR obtained by integrating to a constant depth (Fig. 9a ⊙) was highly variable and was poorly correlated to the NHF. However, the HSR obtained by integrating to a constant isotherm (Fig. 9b ⊙) was predominantly seasonally variable and well correlated to the NHF.

The demeaned climatologies of the HSR, calculated using a constant isotherm, covaried with the NHF. Most of the geographic variability in the seasonal climatology was observed in the magnitude of the seasonal cycle. The range of values decreased with latitude, being largest in the north and smallest near the equator. At higher latitudes, the climatologies had a seasonal winter minimum and summer maximum. Near the equator, a semiannual cycle was observed with maximums in the spring and fall and minimums in the summer and winter. Seasonal motion of the sun primarily controlled the north–south variability of the magnitude in the seasonal variability for all regions. An east–west variability was also observed. The seasonal cycle in the western part of the ocean had larger amplitudes because of the seasonal latent and sensible heat flux associated with wintertime enhancement of air–sea interaction over the western boundary currents.

The differences in the NHF and HSR for a large portion of the North Pacific had a semiannual signal (Fig. 10 ⊙). This semiannual variability may be caused by the seasonal fluctuations in the horizontal advection of heat, which cannot be estimated at this time. Ekman heat transport estimates (not shown) did not account for the semiannual signal in the differences. A comparison of the regional (20° to 55°N, 180° to 115°W) mean difference between the demeaned NHF and HSR seasonal climatologies obtained before and after normalizing each of the temperature profiles to the local 300-m mean temperature showed that normalization of the temperature profiles reduced the rms of the difference from about 40 to 20 W m^{-2}.

5. Annual mean net heat flux and heat storage rates

Annual means for both the HSR and NHF estimates were calculated by averaging the seasonal climatology from each 5° × 5° grid region that contained a full 12-month seasonal climatology. The mean of the seasonal climatology was used rather than the mean of the time series in order to remove any seasonal sampling bias in the dataset. Oceanographic data density is generally larger in the summer months, especially at high latitudes.

The annual mean HSR in the ocean were near zero because the temperature in the ocean did not vary much from year to year when averaged over decadal scales. However, this was not true for the annual NHF (Fig. 11 ⊙). In the western region of the North Pacific, more than 100 W m^{-2} is lost to the atmosphere. A zero NHF contour line runs from the northern coast of Japan southeast to parallel along the coastline of Mexico. To the north of the zero contour line, heat is gained by the ocean at a rate of about 25 W m^{-2}. To the south of the zero contour line, in a wide band, heat is lost to the atmosphere at a rate of about 25 W m^{-2}.

6. Uncertainty analysis

The uncertainty in calculating the seasonal climatology in the heat budget for the North Pacific resulted primarily from the sparse number of temperature profiles in the study's 40-yr time period (1950 to 1990). Errors associated with the HSR calculations are derived from a number of sources. Spatial averaging can introduce a significant amount of error when observations are sparse. Given the low number of temperature profile observations per 5° × 5° grid per month, errors can arise from grouping geographically dispersed data into the 5° × 5° grid and from mesoscale variability. As an example, the variability of the mean temperature profile ‹T_a› within a 5° × 5° grid can be about 5°C. Because of this, all ‹T_a› estimates with large standard deviations and low numbers of observations were removed from the heat storage rate calculation. Another source of error was the effect of spatial bias in the collection of the XBT data. Ship tracks through any one 5° × 5° grid over one month can add error to the ‹T_a› estimate by traveling through either the northern or southern portion of a 5° × 5° grid. Fewer observations increase the potential for error. However, assuming this error is random over each year due to changes in ship tracks, it should be restricted to the monthly mean dataset and should not affect the seasonal climatology. This may not be true in the far northern stations during the winter periods, where seasonal ice cover limits the ship's path to more southerly waters. Other sources of error exist but are not significant. The largest measurement error in the data comes from the XBT probes and is about ±0.05°C (Roemmich and Cornuelle 1987). Average temperatures in the North Pacific are about 10°C, which makes the measurement error small (0.5%). Another source of error is caused by the variations in drop speed of the XBT through the water (Rual et al. 1994). At 100 m, the average depth of the isotherm to which the temperature profiles were integrated, the error is about 2 m, again a small error (2%).

Errors in the NHF estimates arise from biases in the latent and sensible heat flux bulk coefficient estimates and errors in estimating the mean climate parameters, such as cloud cover, sea surface and air temperature, wind speed, and relative humidity. Errors also arise from the sensitivity of the latent heat flux approximations in the western boundary regions and the equatorial regions (Liu and Niiler 1990). In addition to this, the intraannual and interannual variability makes the estimates of the uncertainty in the NHF and HSR seasonal climatology even more difficult to obtain.

The total variability within the individual time series is due to errors in estimation and intraannual and interannual variability. Intraannual and interannual variability can only add to the variance caused by the errors in estimation. The maximum error of the estimate (or uncertainty) in the seasonal climatology for the NHF, HSR, and difference between the NHF and HSR was calculated using the differences between the seasonal climatologies and the individual monthly estimates. As an example, the uncertainty estimate for the NHF seasonal climatology,

$$\epsilon = \frac{2}{\sqrt{n(n-1)}} \sqrt{\sum_{i=1}^{n} (NHF_i - NHF_{clim}^2)}, \quad (9)$$

where n is the number of months of data and clim denotes the monthly mean seasonal climatology. The results of using this formulation to estimate the uncertainty of the seasonal climatology in the NHF, HSR, and difference between the NHF and HSR are shown in Fig. 12 ⊙. The uncertainty shown corresponds to the 95% C.I. for a normally distributed variable.

The largest uncertainty for the NHF occurs in the northwest region of the North Pacific. For most of the North Pacific the estimated seasonal climatology is within 10 W m^{-2} of the true seasonal climatology. The largest uncertainty in the HSR was also in the northwest region of the North Pacific. A region of higher uncertainty occurred in the area parallel to the Kuroshio. This region of higher uncertainty results from the variability in the position of the Kuroshio Front. For both the NHF and HSR, the regions of high uncertainty in the northwest were caused by the high variance in those regions and the low sample numbers. Finally, the uncertainty in the difference between the demeaned NHF and HSR estimates (which is an estimate of how well the seasonal cycle of the NHF and HSR are locally balanced) was similar to that obtained by the HSR uncertainty calculation.

7. North Pacific net northward heat transport

Over decadal timescales, the annual mean NHF is balanced by the annual mean horizontal advection and diffusion of heat. Restated, this means that the local net heat flux is balanced by the local convergence in the horizontal transport of heat over the vertical extent of the water column. By assuming that the flow of heat through the Bering Strait contributes little to the heat balance in the North Pacific, and the heat flux across the ocean–land boundary is insignificant, the annual mean NHF estimates from the northern part of the North Pacific basin to the equator can be spatially integrated to estimate the northward heat transport (NHT) as a function of latitude. Regions of missing data were assumed to have a zero net heat flux. The results of this calculation for this study and several previous heat flux estimates are shown in Fig. 13 ⊙. In conjunction with the estimated northward heat transport curves, the estimated northward heat transport at 47°N and 35°N from Roemmich and McCallister (1989) and the mean and standard error of the heat transport calculated at 24° (Bryden et al. 1991), 10° (Wijffels et al. 1996), and 10°N, 24°N, and 47°N (Macdonald and Wunsch 1996) are also shown. The northward heat transport across the equator was estimated to be about 0.4 petawatts. The estimate agreed well with that measured at 24°N by Wijffels et al. (1996); but it did not agree as well with that estimated by Bryden et al. (1991) at 24°N.

Previous comparisons between these estimates have been difficult because the potential systematic errors from these calculations are cumulative and the resulting estimated envelope from the systematic errors is large enough to encompass all of both estimated and measured heat transport curves and latitude-specific estimates (Talley 1984). However, because the errors associated with annual mean heat flux also affect the seasonal cycle, the difference between the seasonal cycles of the net heat flux and heat storage rates was used as an estimate of the basin-scale systematic error. The assumption here was that the seasonal cycle of the NHF was locally stored and that the effect of the seasonal horizontal heat transport was minimal. A systematic error or bias was not anticipated in the HSR estimates because the estimates were calculated from direct observations, which had small known measurement errors (~ 2%). Therefore, a systematic error, ϵ, was calculated for the NHF from the differences in the demeaned seasonal cycles of the NHF, NHF′, and HSR, HSR′ as

$$\epsilon = \overline{NHF'/HSR'} - 1. \quad (10)$$

This basin-scale systematic error could then be used with the annual mean field of the NHF to integrate the systematic error of the northward heat transport estimate over the North Pacific. In practice, the basin-averaged bias ϵ was estimated using standard principal component analysis techniques (Preisendorfer 1988) with the demeaned climatologies from the NHF and HSR in the North Pacific. Using this technique, a bias of 7% in the annual mean net heat flux was observed (Fig. 14a ⊙). This 7% bias was then used with the annual mean net heat flux and the calculated 20 W m^{-2} rms error in the difference between the seasonal net heat flux and heat storage rates to calculate an error envelope for the annual mean northward heat transport in the North Pacific (Fig. 13 ⊙). As an example of the decrease in magnitude of the bias with the new NHF estimates, a bias of 33% was observed when the seasonal NHF was estimated using the Large and Pond (1982) latent and sensible heat estimates and the Reed (1977) cloud correction (Fig. 14b ⊙).

8. Discussion and conclusions

A new estimate of the heat budget for the North Pacific Ocean that used a combination of measured ocean and atmospheric data is presented. This new heat budget differs from previous estimates in several ways. First, by comparing the seasonal climatological estimates of the NHF and HSR using several different bulk transfer coefficient schemes, it was possible to choose the transfer coefficient scheme that contained the least amount of bias and variance between the schemes tested. The changes in bias and variance observed was primarily due to the latent heat flux estimates (Fig. 5 ⊙) but not the sensible heat flux estimates (Fig. 6 ⊙).

Second, the shortwave solar radiation estimate for the 40-yr time series was obtained from a simple shortwave irradiance model (Bird 1984) with a spatially dependent cloud correction formulation that was parameterized using remotely sensed solar shortwave estimates from Bishop and Rossow (1991). All previous heat budget estimates used cloud correction formulations calibrated to locally obtained datasets. These datasets measure local rather than regional mean values. The use of the Bishop and Rossow (1991) shortwave dataset allowed us to calibrate a cloud correction formulation using a

synoptically derived dataset.

Third, the HSR estimates were obtained by integrating each of the temperature profiles down to a chosen isotherm. This isotherm was chosen to be one degree less than the coldest locally observed sea surface temperature. The chosen isotherm was regarded as the local winter ventilation isotherm. Other methods employed to estimate the NHF use constant depths (White and Cayan 1997, submitted to *J. Geophys. Res.*) or a spatially constant isotherm (Yan et al. 1995) to calculate the HSR. As shown in Fig. 9a 〇⚊, the seasonal climatology of the HSR (obtained by integrating the temperature profiles down to 300 m) compared poorly to the seasonal climatology of the NHF estimates. Integrating to a constant isotherm resulted in seasonal HSR climatologies that were very similar to the seasonal climatologies of the NHF (Fig. 9b 〇⚊). Also, it is interesting to note that while both the time series of the monthly mean vertically averaged temperature $\langle T_a \rangle$ and isotherm depth $\langle h \rangle$ were sensitive to the isotherm chosen, the resulting time series of the heat storage rate $\rho c_p \langle h \rangle (\partial \langle T_a \rangle / \partial t)$ was not.

The most significant result from this new heat budget was that for most regions in the North Pacific the seasonal climatologies of the NHF and HSR were locally balanced. The greatest difference between the seasonal climatologies of the NHF and HSR occurred in the western boundary current region. This increased difference was primarily attributed to the large meanders associated with the Kuroshio and Kuroshio Extension, which meander into preferential patterns (Mizuno and White 1983) and thus cause error in the estimate of the HSR. The seasonal variability in the horizontal transport of heat may be another potential source of the difference between the seasonal climatologies of the NHF and HSR. This source of error can affect the balance between the NHF and HSR in other regions of the Pacific.

The difference between the seasonal climatology of the NHF and HSR in this region had a distinct semiannual signal. By normalizing the temperature profiles in the northeastern portion of the North Pacific to the local 300-m mean temperature, the rms in the difference between the seasonal climatologies of the NHF and HSR was reduced by half, from 40 to 20 W m^{-2}. This semiannual difference may be caused by the seasonal variability in the horizontal advection of heat. However, given the crude parameterizations involved in the NHF estimates, it is difficult to make such a conclusion. Finally, by carefully choosing among the wide variety of available methods for estimating the latent and sensible heat flux and using a new cloud parameterization to calculate the shortwave irradiance, we were able to reduce the bias between the seasonal NHF and HSR estimates from about 33% to 7%.

This estimate of the annual mean northward heat transport agrees with three of the four direct estimates available in the literature. However, only three of those estimates contain error estimates of the calculation; and, in all of those estimates, the error is quite large. Because the comparison between the seasonal cycle of the NHF and HSR estimates demonstrated a bias of only 7%, the confidence in the heat transport estimate is greater since it has a much smaller error envelope than previous error estimates (Talley 1984). However, because of the lack of data in the equatorial regions of the North Pacific, the estimates of the heat transport in that area may be too high. There are at present no direct estimates of the northward heat transport in this region with which to compare these results.

This study used data from the NODC archives to obtain temperature data and the COADS to obtain the climate observations. There are other sources of data available to use in calculating the NHF and HSR. This study only focused on the COADS and NODC data.

Results from this study can now be used in several areas of oceanography. The correct seasonal NHF can be used to force mixed layer models. The new cloud parameterization can be used to estimate the solar irradiance. And, because most of the regions on the North Pacific were shown to be seasonally balanced between the NHF and HSR, the implementation of 1D models to these areas should be appropriate for studying the seasonal cycle of the mixed layer.

REFERENCES

Bird, R. E., 1984: A simple, solar spectral model for direct-normal and diffuse horizontal irradiance. *Sol. Energy,* **32,** 461–471..

Bishop, J. K. B., and W. B. Rossow, 1991: Spatial and temporal variability of global surface solar irradiance. *J. Geophys. Res.,* **96,** 16839–16858..

Blanc, T. V., 1985: Variation of bulk-derived surface flux, stability, and roughness results due to the use of different transfer coefficient schemes. *J. Phys. Oceanogr.,* **15,** 650–669..

Bryden, H. L., D. H. Roemmich, and J. A. Church, 1991: Ocean heat transport across 24°N in the Pacific. *Deep-Sea Res.,* **38,** 297–324..

Bunker, A. F., 1976: Computations of surface energy flux and annual air–sea interaction cycles of the North Atlantic Ocean. *Mon. Wea. Rev.,* **104,** 1122–1140.. Find this article online

Cayan, D. R., 1992a: Variability of latent and sensible heat fluxes estimated using bulk formulae. *Atmos.-Oceans,* **30,** 1–42..

— ,1992b: Latent and sensible heat flux anomalies over the northern oceans: The connection to monthly atmospheric circulation. *J. Climate,* **5,** 354–369..

— ,1992c: Latent and sensible heat flux anomalies over the northern oceans: Driving the sea surface temperature. *J. Phys. Oceanogr.,* **22,** 829–881..

Chertock, B., R. Frouin, and C. Gautier, 1992: A technique for global monitoring of net solar irradiance at the ocean surface. Part II:Validation. *J. Appl. Meteor.,* **31,** 1067–1083.. Find this article online

Dobson, F. W., and S. D. Smith, 1988: Bulk models of solar radiation at sea. *Quart. J. Roy. Meteor. Soc.,* **114,** 165–182..

Emery, W., 1976: The role of vertical motion in the heat budget of the upper northeastern Pacific Ocean. *J. Phys. Oceanogr.,* **6,** 299–305..

Esbensen, S. K., and V. Kushnir, 1981: The heat budget of the global ocean: An atlas based on estimates from surface marine observations. Climate Research Institute, Rep. No. 29, Oregon State University, 27 pp. and 188 figs. [Available from College of Oceanic and Atmospheric Sciences, Oregon State University, Corvallis, OR 97331.].

— ,and R. W. Reynolds, 1981: Estimating monthly averaged air–sea transfers of heat and momentum using the bulk aerodynamic method. *J. Phys. Oceanogr.,* **11,** 457–465..

Fissel, D. B., S. Pond, and M. Miyake, 1977: Computation of surface fluxes from climatological and synoptic data. *Mon. Wea. Rev.,* **105,** 26–36.. Find this article online

Frouin, R., and B. Chertock, 1992: A technique for global monitoring of net solar irradiance at the ocean surface. Part I: Model. *J. Appl. Meteor.,* **31,** 1056–1066.. Find this article online

Gill, A. E., and P. P. Niiler, 1973: The theory of the seasonal variability in the ocean. *Deep-Sea Res.,* **20,** 141–177..

Hansen, D. V., and C. A. Paul, 1984: Genesis and effects of long waves in the Equatorial Pacific. *J. Geophys. Res.,* **89,** 10431–10440..

Hastenrath, S., and P. J. Lamb, 1977: *Climate Atlas of the Tropical Atlantic and Eastern Pacific Oceans.* University of Wisconsin Press, 105 pp..

— ,and — ,1978: *Heat Budget Atlas of the Tropical Atlantic and Eastern Pacific Oceans.* University of Wisconsin Press, 104 pp..

Hsiung, J., 1985: Estimates of global oceanic meridional heat transport. *J. Phys. Oceanogr.,* **15,** 1405–1413..

Isemer, H.-J., and L. Hasse, 1987: *The Bunker Climate Atlas of the North Atlantic Ocean.* Vol. 2. *Air–Sea Interactions.* Springer-Verlag, 218 pp..

Kenyon, K. E., 1983: Property differences in the central northeastern Pacific between April 1976 and July 1977. *J. Oceanogr. Soc. Japan,* **39,** 73–81..

Large, W. G., and S. Pond, 1982: Sensible and latent heat flux measurements over the ocean. *J. Phys. Oceanogr.,* **12,** 464–482..

Ledvina, D. V., G. S. Young, R. A. Miller, and C. W. Fairall, 1993:The effect of averaging on bulk estimates of heat and momentum fluxes for the tropical western Pacific Ocean. *J. Geophys. Res.,* **98,** 20211–20217..

Liu, W. T., and P. P. Niiler, 1990: The sensitivity of latent heat flux to the air humidity approximations used in ocean circulation models. *J. Geophys. Res.,* **95,** 9745–9753..

— ,K. B. Katsaros, and J. A. Businger, 1979: Bulk parameterizations of air–sea exchanges of heat and water vapor including molecular constraints at the interface. *J. Atmos. Sci.,* **36,** 1722–1735.. Find this article online

— ,W. Tang, and F. J. Wentz, 1992: Precipitable water and surface humidity over global oceans from Special Sensor Microwave/Imager and European Center for Medium-Range Weather Forecasts. *J. Geophys. Res.,* **97,** 2251–2264..

Macdonald, A. M., and C. Wunsch, 1996: Oceanic estimates of global ocean heat transport. U. S. WOCE Rep. 8, 64 pp. [Available from U.S. WOCE Office, Dept. of Oceanography, Texas A&M University, College Station, TX 77843.].

Mizuno, K., and W. White, 1983: Annual and interannual variability in the Kuroshio Current System. *J. Phys. Oceanogr.,* **13,** 1847–1867..

Oberhuber, J. M., 1988: An atlas based on the 'COADS' data set: The budgets of heat, buoyancy and turbulent kinetic energy at the surface of the global ocean. Max-Planck-Institute for Meteorology, Rep. 15, 20 pp..

Payne, R. E., 1972: Albedo of the sea surface. *J. Atmos. Sci.,* **29,** 959–970.. Find this article online

Preisendorfer, R. W., 1988: *Principal Component Analysis in Meteorology and Oceanography.* posthumously compiled and edited by C. D. Mobley, Elsevier, 425 pp..

Reed, R. K., 1977: On estimating insolation over the ocean. *J. Phys. Oceanogr.,* **7,** 482–485..

Roemmich, D., and B. Cornuelle, 1987: Digitization and calibration of the expendable bathythermograph. *Deep-Sea Res.,* **34,** 299–307..

— , and T. McCallister, 1989: Large scale circulation of the North Pacific Ocean. *Progress in Oceanography,* Vol. 22, Pergamon 171–204..

Rossow, W. B., F. Mosher, E. Kinsell, A. Arking, M. Desbois, E. Harrison, P. Minnis, E. Ruprecht, G. Seze, C. Simmer, and E. Smith, 1985: ISCCP cloud algorithm intercomparison. *J. Climate Appl. Meteor.,* **24,** 877–903..

Rual, P., K. Hanawa, R. Bailey, A. Sy, and M. Szabados, 1994: New depth equation for commonly used expendable bathythermographs Sippican and TSK T-4, T-6 and T-7 probes. *Int. WOCE Newslett.,* **17,** 13–16..

Schlatter, T. W., and D. V. Baker, 1981: *Algorithms for Thermodynamic Calculations.* NOAA/ERL PROFS Program Office, 37 pp..

Semtner, A. J., and R. M. Chervin, 1992: Ocean general circulation from a global eddy-resolving model. *J. Geophys. Res.,* **97,** 5493–5550..

Slutz, R. J., S. J. Lubker, J. D. Woodruff, R. L. Jenne, D. H. Joseph, P. M. Steurer, and J. D. Elms, 1985: Comprehensive Ocean–Atmosphere Data Set: Release I. NOAA Environmental Research Laboratories, Climate Research Program, 268 pp..

Smith, S. D., and F. W. Dobson, 1984: The heat budget at ocean weather station BRAVO. *Atmos.–Ocean,* **22,** 1–22..

Stevenson, J. W., and P. P. Niiler, 1983: Upper ocean heat budget during the Hawaii-to-Tahiti shuttle experiment. *J. Phys. Oceanogr.,* **13,** 1894–1907..

Stockdale, T., D. Anderson, M. Davey, P. Delecluse, A. Kattenberg, Y. Kitamura, M. Latif, and T. Yamagata, 1993: Intercomparison of tropical ocean GCMS. Report of the TOGA Numerical Experimentation Group, World Climate Research Programme, WCRP-79, WMO/TD-No. 45, 79 pp..

Suga, T., and K. Hanawa, 1990: The mixed-layer climatology in the northwest part of the North Pacific subtropical gyre and the formation area of the Subtropical Mode Water. *J. Mar. Res.,* **48,** 543–566..

Talley, L. D., 1984: Meridional heat transport in the Pacific Ocean. *J. Phys. Oceanogr.,* **14,** 231–241..

Wijffels, S. E., J. M. Toole, H. L. Bryden, R. A. Fine, W. J. Jenkins, and J. L. Bullister, 1996: The water masses and circulation at 10°N in the Pacific. *Deep-Sea Res.,* **43,** 501–544..

Woodruff, S. D., R. J. Slutz, R. L. Jenne, and P. M. Steurer, 1987: A Comprehensive Ocean–Atmosphere Data Set. *Bull. Amer. Meteor. Soc.,* **68,** 1239–1250.. Find this article online

Wyrtki, K., 1965: The average annual heat balance of the North Pacific and its relation to ocean circulation. *J. Geophys. Res.,* **70,** 4547–4559..

Yan, X.-H., P. P. Niiler, S. K. Nadiga, R. Stewart, and D. Cayan, 1995:The seasonal heat storage in the North Pacific: 1979–1989. *J. Geophys. Res.,* **100,** 6899–6926..

APPENDIX

9. Heat Conservation Equation

a. Heat storage rate

Because of the role that vertical motion plays in the upper-ocean heat budget (Emery 1976), a heat storage rate equation was chosen that calculated the amount of heat stored down to a chosen isotherm. Here is a formal derivation of this heat storage rate equation.

We begin with the conservation of mass equation,

$$\frac{\partial u}{\partial x} + \frac{\partial v}{\partial y} + \frac{\partial w}{\partial z} = 0, \qquad \text{(A1)}$$

and the conservation of heat equation,

$$\rho c_p \left[\frac{\partial T}{\partial t} + u\frac{\partial T}{\partial x} + v\frac{\partial T}{\partial y} + w\frac{\partial T}{\partial z} \right] = \frac{\partial q}{\partial z}, \qquad \text{(A2)}$$

where ρ, c_p, and T are the mean density, specific heat, and temperature of seawater, respectively, and q is the vertical

heat flux. By multiplying Eq. (A1) by T and dividing Eq. (A2) by ρc_p, we can add both equations to get

$$\left[\frac{\partial T}{\partial t} + \frac{\partial uT}{\partial x} + \frac{\partial vT}{\partial y} + \frac{\partial wT}{\partial z}\right] = \frac{1}{\rho c_p}\frac{\partial q}{\partial z}. \qquad (A3)$$

Integrating Eq. (A3) from the surface down to some chosen time- and space-dependent isotherm, $h = f(x, y, t)$, yields

$$\int_{-h}^{0}\left[\frac{\partial T}{\partial t} + \frac{\partial uT}{\partial x} + \frac{\partial vT}{\partial y} + \frac{\partial wT}{\partial z} = \frac{1}{\rho c_p}\frac{\partial q}{\partial z}\right] dz. \qquad (A4)$$

The horizontal heat divergence terms can be rewritten as follows:

$$\int_{-h}^{0}\frac{\partial}{\partial x}uT\ dz = \frac{\partial}{\partial x}\int_{-h}^{0} uT\ dz - u_{-h}T_{-h}\frac{\partial h}{\partial x}, \qquad (A5)$$

and

$$\int_{-h}^{0}\frac{\partial}{\partial y}vT\ dz = \frac{\partial}{\partial y}\int_{-h}^{0} vT\ dz - v_{-h}T_{-h}\frac{\partial h}{\partial y}. \qquad (A6)$$

Substituting Eqs. (A5) and (A6) into Eq. (A4) and adding the following equalities:

$$\frac{\partial}{\partial x}u_a\int_{-h}^{0} T\ dz = \int_{-h}^{0} u\ dz\,\frac{\partial T_a}{\partial x} + T_a\frac{\partial}{\partial x}\int_{-h}^{0} u\ dz \qquad (A7)$$

and

$$\frac{\partial}{\partial y}v_a\int_{-h}^{0} T\ dz = \int_{-h}^{0} v\ dz\,\frac{\partial T_a}{\partial y} + T_a\frac{\partial}{\partial y}\int_{-h}^{0} v\ dz, \qquad (A8)$$

where

$$T_a = \frac{1}{h}\int_{-h}^{0} T\ dz,$$

$$u_a = \frac{1}{h}\int_{-h}^{0} u\ dz,$$

$$v_a = \frac{1}{h}\int_{-h}^{0} v\ dz,$$

are the vertically averaged temperature and horizontal velocity terms, respectively, which yields

$$\int_{-h}^{0}\frac{\partial T}{\partial t}dz + \frac{\partial}{\partial x}\int_{-h}^{0} uT\ dz - u_{-h}T_{-h}\frac{\partial h}{\partial x} + \int_{-h}^{0} u\ dz\,\frac{\partial T_a}{\partial x} + T_a\frac{\partial}{\partial x}\int_{-h}^{0} u\ dz - \frac{\partial}{\partial x}u_a\int_{-h}^{0} T\ dz + \frac{\partial}{\partial y}\int_{-h}^{0} vT\ dz$$

$$- v_{-h}T_{-h}\frac{\partial h}{\partial y} + \int_{-h}^{0} v\ dz\,\frac{\partial T_a}{\partial y} + T_a\frac{\partial}{\partial y}\int_{-h}^{0} v\ dz - \frac{\partial}{\partial y}v_a\int_{-h}^{0} T\ dz + \int_{-h}^{0}\frac{\partial}{\partial z}wT\ dz = \frac{1}{\rho c_p}\int_{-h}^{0}\frac{\partial q}{\partial z}dz. \qquad (A9)$$

(Click the equation graphic to enlarge/reduce size)

The depth-integrated conservation of mass equation,

$$\int_{-h}^{0}\left[\frac{\partial u}{\partial x} + \frac{\partial v}{\partial y} + \frac{\partial w}{\partial z} = 0\right] dz, \qquad (A10)$$

can be rewritten as

$$w_{-h} = \frac{\partial}{\partial x} \int_{-h}^{0} u \ dz + \frac{\partial}{\partial y} \int_{-h}^{0} v \ dz - u_{-h} \frac{\partial h}{\partial x} - v_{-h} \frac{\partial h}{\partial y}.$$

(A11)

With this equation, we can rewrite the term

$$T_a w_{-h} = T_a \frac{\partial}{\partial x} \int_{-h}^{0} u \ dz + T_a \frac{\partial}{\partial y} \int_{-h}^{0} v \ dz$$

$$- T_a u_{-h} \frac{\partial h}{\partial x} - T_a v_{-h} \frac{\partial h}{\partial y}.$$

(A12)

Also, we can rewrite the depth-integrated vertical heat advection term as

$$\int_{-h}^{0} \frac{\partial}{\partial z} wT \ dz = -w_{-h} T_{-h}.$$

(A13)

Substituting both Eqs. (A12) and (A13) into Eq. (A9) yields

$$\int_{-h}^{0} \frac{\partial T}{\partial t} \ dz + \int_{-h}^{0} u \ dz \frac{\partial T_a}{\partial x} + \frac{\partial}{\partial x} \int_{-h}^{0} uT \ dz - \frac{\partial}{\partial x} T_a \int_{-h}^{0} u \ dz + T_a u_{-h} \frac{\partial h}{\partial x} - u_{-h} T_{-h} \frac{\partial h}{\partial x} + \int_{-h}^{0} v \ dz \frac{\partial T_a}{\partial y}$$

$$+ \frac{\partial}{\partial y} \int_{-h}^{0} vT \ dz - \frac{\partial T_a}{\partial y} \int_{-h}^{0} v \ dz + T_a v_{-h} \frac{\partial h}{\partial y} - v_{-h} T_{-h} \frac{\partial h}{\partial y} + T_a w_{-h} - w_{-h} T_{-h} = \frac{1}{\rho c_p} \int_{-h}^{0} \frac{\partial q}{\partial z} \ dz.$$

(A14)

(Click the equation graphic to enlarge/reduce size)

The local depth-integrated time derivative can be rewritten as

$$\int_{-h}^{0} \frac{\partial T}{\partial t} \ dz = h \frac{\partial T_a}{\partial t} + T_a \frac{\partial h}{\partial t} - T_{-h} \frac{\partial h}{\partial t}.$$

(A15)

Substituting Eq. (A15) and adding the following equalities,

$$\frac{\partial}{\partial x} \left[u_a T_a \int_{-h}^{0} \ dz \right] = \frac{\partial}{\partial x} \left[u_a \int_{-h}^{0} T \ dz \right]$$

(A16)

and

$$\frac{\partial}{\partial y} \left[v_a T_a \int_{-h}^{0} \ dz \right] = \frac{\partial}{\partial y} \left[v_a \int_{-h}^{0} T \ dz \right],$$

(A17)

to (A14) gives

$$+ (T_a - T_{-h})\left(\frac{\partial}{\partial t} + u_{-h}\frac{\partial}{\partial x} + v_{-h}\frac{\partial}{\partial y} + w_{-h}\right)$$

$$= \frac{q_0 - q_{-h}}{\rho c_p}. \qquad (A18)$$

The equation can be further rewritten as

$$h\frac{\partial T_a}{\partial t} + h\mathbf{v}_a\cdot\nabla T_a + \nabla\cdot\left(\int_{-h}^{0}\hat{\mathbf{v}}\hat{T}\,dz\right) + (T_a - T_{-h})$$

$$\times\left(\frac{\partial h}{\partial t} + \mathbf{v}_{-h}\cdot\nabla h + w_{-h}\right) = \frac{q_0 - q_{-h}}{\rho c_p}, \qquad (A19)$$

where $\hat{\mathbf{v}}$ is the deviation from the vertically averaged horizontal velocity ($\mathbf{v} = \mathbf{v}_a + \hat{\mathbf{v}}$), and $\hat{T}$ is the deviation from the vertically averaged temperature ($T = T_a + \hat{T}$).

This study follows the logic of Stevenson and Niiler (1983). The depth that the temperature profile is integrated, $h = f(x, y, t)$, is always below the main thermocline. Therefore, the flux of heat through the bottom q_{-h} is negligible, and the surface that h comprises behaves similar to a material surface. Because of this, the entrainment rate of heat across this interface is small and so the term ($\partial h/\partial t + \mathbf{v}_{-h}\cdot\nabla h + w_{-h}$) can be neglected. The horizontal eddy heat transport terms are also neglected since this term has a very small seasonal signal (Gill and Niiler 1973) and mainly balances the net annual heat flux. Mesoscale ocean heat transport has been shown to be significant only within ±5° of the equator (Hansen and Paul 1984).

The final equation contains a heat storage rate term, a horizontal heat advection term, and a net heat flux term:

$$\rho c_p\left(h\frac{\partial T_a}{\partial t} + h\mathbf{v}_a\cdot\nabla T_a\right) = Q_{net}, \qquad (A20)$$

where $Q_{net} = q_0$ is the net heat flux across the ocean surface.

Figures
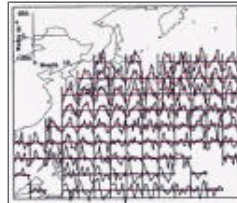
Click on thumbnail for full-sized image.

Fig. 1. Climatologies of the heat storage rates obtained by integrating the temperature profiles down to 300 m (blue) and the isotherm whose temperature is one degree less than the coldest observed SST for that grid region (red). The individual plots are drawn over the 5° × 5° grid region from where the temperature profile data was obtained.
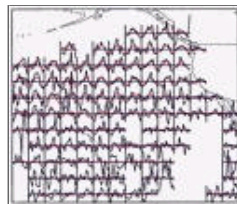
Click on thumbnail for full-sized image.

Fig. 1. (*Continued*)

Fig. 2. Sensitivity of (a) $\rho c_p \langle h \rangle (\partial \langle T_a \rangle / \partial t)$, (b) $\langle T_a \rangle$, and (c) $\langle h \rangle$ to changes in the choice of isotherm (3°–6°C, by 1° increments) down to which the temperature profile (XBT/CTD) data were integrated. The time series presented here used data obtained from the 45°–50°N, 145°–140°W region.
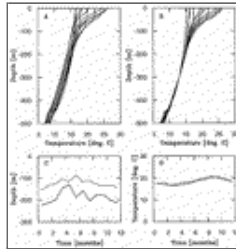
Fig. 3. The mean monthly temperature profiles from the 35°–40°N, 165°–170°E bin (a) before and (b) after normalization of each profile to the mean 300-m temperature. The time series of (c) $\langle h \rangle$ and (d) $\langle T_a \rangle$ for before (solid) and after (hatched) normalization are shown.
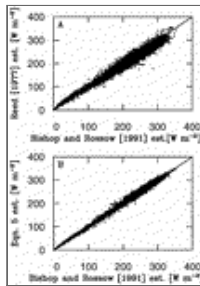
Fig. 4. Comparison of the climatological values for the solar shortwave irradiance flux at the ocean surface between the Bishop and Rossow (1991) dataset and the Bird (1984) solar irradiance model with COADS cloud data and the (a) Reed (1977) and (B) nonlinear [Eq. (5)] cloud correction.
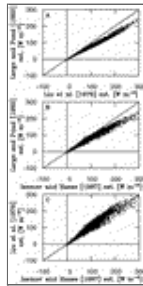
Fig. 5. An intercomparison of the climatological latent heat flux estimates obtained from the bulk formulas of Large and Pond (1982), Liu et al. (1979), and Isemer and Hasse (1987).
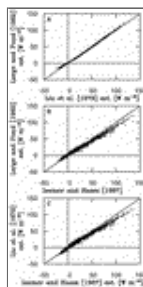
Fig. 6. An intercomparison of the climatological sensible heat flux estimates obtained from the bulk formulas of Large and Pond (1982), Liu et al. (1979), and Isemer and Hasse (1987).
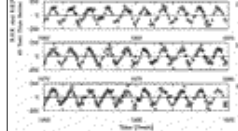
Fig. 7. The climatologies (upper panel) of the net heat flux (solid line) and heat storage rates (dashed line) derived from the individual monthly mean values of the NHF (diamonds) and HSR (circles) from the 40-yr (1950 to 1990) time series (lower panels) for OWS Papa.
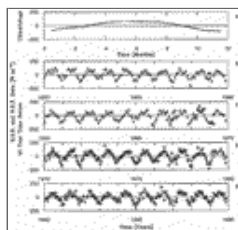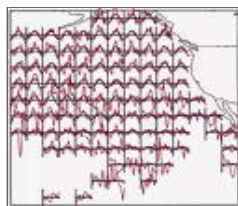
Fig. 8. As in Fig. 7 ⊙= but to OWS November.
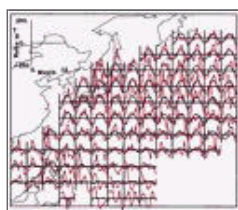
Fig. 9. Climatologies of the demeaned net heat flux (blue) and heat storage rates (red) obtained by integrating the temperature profiles down to (a) 300 m, (b) the isotherm whose temperature is one degree less than the coldest observed SST for that grid region. The individual plots are drawn over the 5° × 5° grid region from where the temperature data was obtained. All temperature profiles within the outlined blue box (b) were normalized to the local 300-m mean temperature. The region outlined by the blue box (b) is also the region compared in Fig. 10 ⊙=. The black boxes indicate the grid location of OWS Papa and November, whose time series were shown in Figs. 7 ⊙= and 8 ⊙=, respectively.
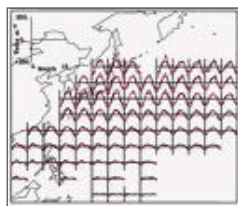
Fig. 9a. (*Continued*)

Fig. 9b. (*Continued*)
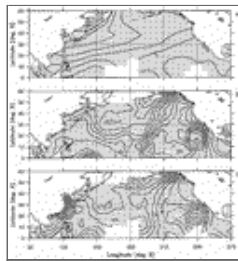
Fig. 9b. (*Continued*)
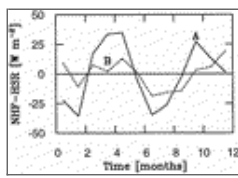
Click on thumbnail for full-sized image.

Fig. 10. Regional (20°–55°N, 180°–115°W) mean difference between the demeaned net heat flux and heat storage rate climatologies obtained by integrating the temperature profiles down to (a) (solid line) the isotherm whose temperature is 1°C colder than the coldest observed SST for that specific 5° × 5° grid region and (b) (dashed line) the same isotherm as in (a) but after normalizing each temperature profile to the local 300-m mean temperature.
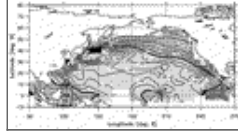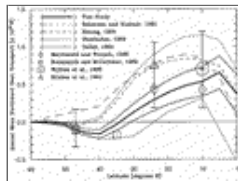

Click on thumbnail for full-sized image.

Fig. 11. The annual mean net heat flux between 1950 and 1990. Contour interval is 10 W m^{-2}. Positive contours: solid line; negative contours: dashed line. Shaded region indicates where data was available.
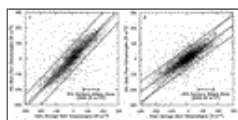

Click on thumbnail for full-sized image.

Fig. 12. Uncertainty estimate for the (a) net heat flux climatology, (b) heat storage rate climatology, and (c) the difference between the demeaned net heat flux and heat storage rate climatologies.

Click on thumbnail for full-sized image.

Fig. 13. The annual mean northward heat transport (petawatts) for the North Pacific obtained by integrating the annual mean net heat flux estimates using data from this study (thick solid line), and the previous studies of Talley (1984), Oberhuber (1988), Hsiung (1985), and Esbensen and Kushnir (1981). The error estimate from this study obtained from an estimated ±20 W m^{-2} rms error and a 7% bias on the annual mean is shown with the thin solid line. The latitude-specific estimates of northward heat transport from Macdonald and Wunsch (1996), Roemmich and McCallister (1989), Bryden et al. (1991), and Wijffels (1995) are also shown.

Click on thumbnail for full-sized image.

Fig. 14. A comparison of the demeaned net heat flux and net heat storage rate climatologies obtained using the latent and sensible heat flux estimates of (a) Liu et al. (1979) and (b) Large and Pond (1988), and the cloud correction from (a) this study and (b) Reed (1977). The angle of the principal component and the variance ellipse (thick curve and solid line) is used to define the amount of bias and error, respectively, between the estimates. The scale of the variance ellipse is shown in the bottom right of the plot. The dashed lines bracket the region encompassing twice the standard deviation of the values about the principal axis.

* Current affiliation: Natural Sciences Division, Southampton College, Long Island University, Southampton, New York.

Corresponding author address: Dr. John R. Moisan, Natural Sciences Division, Southampton College, Long Island University, Southampton, NY

11968.

E-mail: jmoisan@southampton.linnet.edu